13TH CANADIAN MASONRY SYMPOSIUM
HALIFAX, CANADA
JUNE 4TH – JUNE 7TH 2017

RELIABILITY OF UNREINFORCED CONCRETE MASONRY WALLS BOUNDED BY REINFORCED CONCRETE FRAMES

Rahimi, Reza[1]; Fenton, Gordon A.[2] and Liu, Yi[3]

ABSTRACT

This paper presents a study on the probability distribution of the lateral strength of unreinforced masonry (URM) infill walls bounded by reinforced concrete (RC) frames. Based on the load and resistance factor design (LRFD) procedure for URM, the failure probability of the system was studied. The distribution of the lateral strength is a key component of such a probability estimate. To determine this distribution, the compressive strength, f'_m, of the URM infill wall was modeled as a continuous spatially variable random field. Based on f'_m, other mechanical properties of masonry, such as the elastic modulus as well as the ultimate strain and the corresponding stress, were determined using established relationships including a random model error component. A finite element model employing shell elements using the OpenSEES program was used to calculate the lateral strength of the infill and the lateral load vs. displacement behaviour of the infill system. The Monte-Carlo simulation method was then used to produce histograms of lateral strength, over a range of statistics (mean, standard deviation, and correlation length) of f'_m. A fitted strength distribution was then determined and its application in calculation of failure probabilities of the masonry infilled frames was proposed.

KEYWORDS: *reliability-based design, masonry infill, compressive strength, random field*

INTRODUCTION

Masonry walls built inside a steel or RC frame are commonly referred to as masonry infills. The presence of masonry infills has been shown through previous experimental studies [1-4] to have a significant effect on the in-plane response of masonry infilled frames in terms of changing stiffness, strength, and failure mode of the frame system. The accurate evaluation of masonry infill contribution to the frame system behaviour is crucial to a safe and economical design. With the

[1] Research Assistant, Department of Civil and Resource Engineering, Dalhousie University, 5248 Morris St., Halifax, NS, Canada, reza.rahimi@dal.ca
[2] Professor, Department of Engineering Mathematics, Dalhousie University, 5269 Morris St., Halifax, NS, Canada, gordon.fenton@dal.ca
[3] Professor and Department Head, Department of Civil and Resource Engineering, Dalhousie University, 5248 Morris St., Halifax, NS, Canada, yi.liu@dal.ca

advancement of computer technology, recent research effort has increasingly implemented numerical modelling using finite element methods [3-5] as an effective tool to provide results over a wide range of parameters which were often beyond the feasibility of physical tests. These models were mainly encoded using commercial software such as ANSYS and ABAQUS. While these studies demonstrated the capability of computer modelling in the simulation of masonry infilled frames, there was commonly a lack of information provided in existing studies on the input material parameters and analysis procedure, which made them difficult to be adopted by others in their parametric studies.

The Canadian masonry design standard S304 has been using the resistance factor, φ_m, of 0.55 [6] until its 2004 edition in which this factor was increased from 0.55 to 0.6 and has been used since [7]. This resistance factor is applied to the lateral factored resistance of the masonry infilled walls. In order to achieve a reliable design of the masonry infilled walls based on the load and resistance factored design philosophy (LRFD), a reliable lateral load resistance distribution of the infilled wall should be employed.

This paper was then motivated to accomplish two tasks. The first is to develop a numerical model which is capable of simulating the in-plane behaviour of masonry infilled RC frames of varying material and geometric properties, and then to estimate the distribution of the lateral load resistance through the FE model analysis using a random field simulation technique [8]. To the authors' best knowledge, there are no existing studies on random field simulation of compressive strength effect of masonry on lateral resistance of masonry infilled frames. The finite element package OpenSEES, available in the public domain, was used for the modelling. The robustness and computational efficiency make the OpenSEES a strong competitor to other commercial software such as ANSYS and ABAQUS. The model was validated against experimental results of masonry infilled RC frames tested under both static and quasi-static cyclic loading. The FE model was then used to determine the lateral resistance distribution of the masonry infilled frame by implementing random fields of f'_m with different mean values, standard deviations and spatial correlation lengths.

EXPERIMENTAL PROGRAM

Two sets of experiments of concrete masonry infilled RC frames subjected to in-plane loading were conducted in the same research group by Hu [2] and Steeves [5]. While using the same geometry and materials for infilled specimens, one set of experiments was conducted under static loading whereas the other set was conducted under quasi-static loading. The specimens and their associated parameters are summarized in Table 1. The reinforcing steel used in the RC frames of both tests was from the same batch and the yield stress, ultimate stress and Young's modulus were determined to be 446 MPa, 665 MPa, and 247357MPa, respectively. Figure 1 shows the dimensions and reinforcement details used for all specimens. Figure 2 (a) shows a schematic view of the test set-up. A hydraulic actuator was used to apply both static and quasi-static lateral load. The base beam of the frame was clamped to the strong floor and braced using hydraulic jacks to prevent potential in-plane movements. Displacement transducers (LVDTs) were used to measure

the specimen displacement. In the case of quasi-static loading, two threaded rods running the full length of the top beam were installed on the specimens to enable a pulling action on the specimen. During the static test, the lateral load was applied gradually at a rate of 6 kN per minute to the top beam until failure of the specimen. In the cyclic loading test, a sequential phased displacement technique was used to apply the displacement to the infilled frame based on the procedure specified by the Applied Technology Council (ATC 24) for cyclic load test [9]. Figure 2 (b) shows the lateral quasi-static loading protocol where the peak amplitude for each set of cycles is defined based on the yield deformation. The displacement amplitudes were applied at a rate of 10 mm per minute to ensure the quasi-static nature of the loading. The results of this experimental program were used to calibrate the numerical model, as discussed in the following sections.

Table 1: Summary of the Test Specimens

Static Test				Quasi-Static Test				
Spec ID	**Gap**	f'_c **MPa**	f'_m **MPa**	**Spec ID**	**Gap**	**W***	f'_c **MPa**	f'_m **MPa**
BF	N.A.	42.3	-	BF	N.A.	N.A.	29.2	-
IF-NG	-	42.3	16.7	IF-FG12	12 mm Top Gap & 12 mm Side Gap (6 mm each side)	-	29.2	11.1
IF-TG7	7 mm Top Gap	42.3	16.7	IF-W-TG12	12 mm Top Gap	20%	29.2	10.0
IF-TG12	12 mm Top Gap	42.3	16.7	IF-TG25	25 mm Top Gap	-	29.2	11.1
IF-SG7	7 mm Side Gap (3.5 mm each side)	45.3	17.1	IF-W-SG12	12 mm Side Gap (6 mm each side)	20%	29.2	10.0
IF-SG12	12 mm Side Gap (6 mm each side)	45.3	17.1	-	-	-		

* Window Opening/Infill Area Ratio

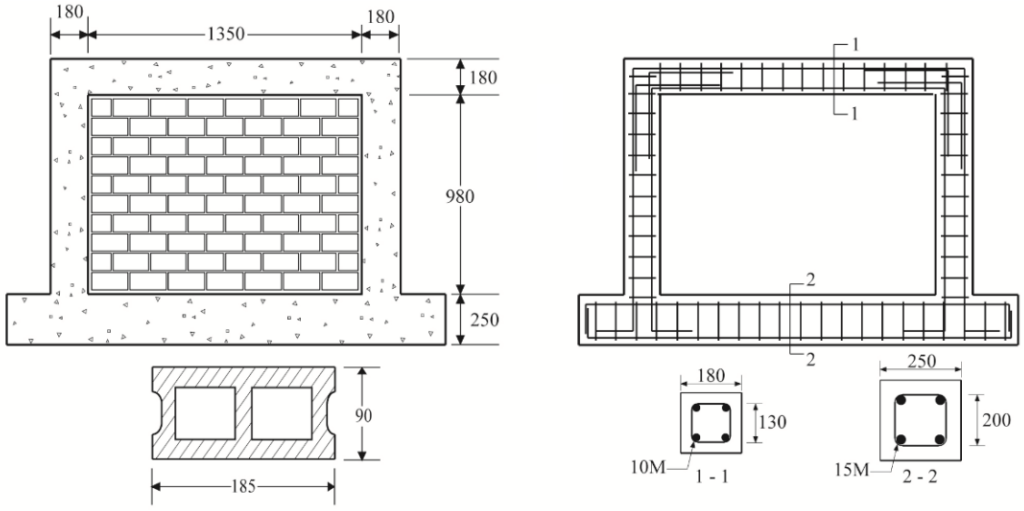

Figure 1: Details of Test Specimen (unit: mm)

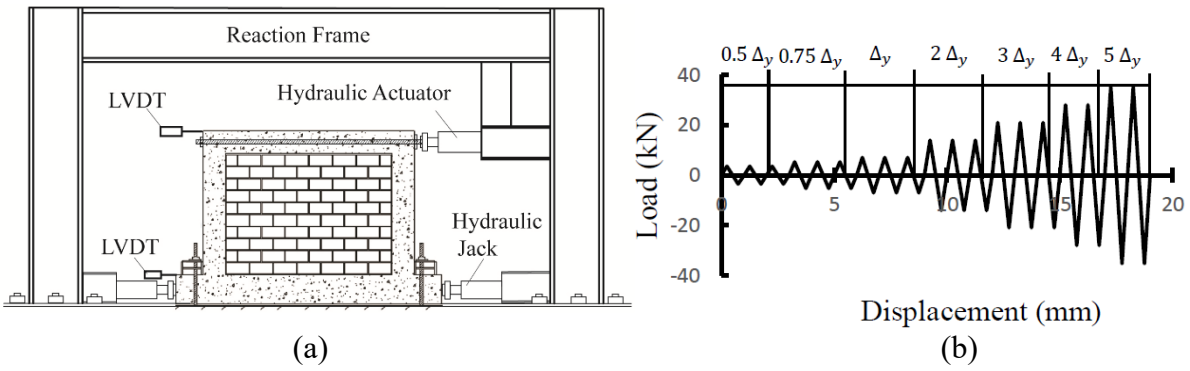

Figure 2: (a) Schematic View of Test Set-Up (b) Loading Protocol for Quasi-Static Loading

NUMERICAL MODELING

The OpenSEES [10] is an open-source object-oriented software program developed primarily for simulation of structural seismic behaviour. It has been successfully used ([11], [12]) to model different aspects of masonry infilled frames. This paper adopted nonlinear beam-column elements and continuum elements to model the RC frame and the infill respectively. The model was developed to accurately simulate the behaviour and predict the ultimate lateral strength of the infilled frame while incorporating various geometric and material properties.

Modelling of the Bare RC Frame

The modelling of RC frame members adopted the fibre element, available in the OpenSEES element library. The fibre element is essentially a two-node beam-column element with 6 degrees of freedom at each node. In this case, the reinforced concrete section was divided into three different segments including the concrete cover, concrete core and steel reinforcement. Figure 3 shows both the fibre discretization and the number of fibres (Nf) of each segment used in the model. A convergence study was conducted on the number of the fibres in each segment and the number of fibres chosen was able to provide accurate results with reasonable computational time.

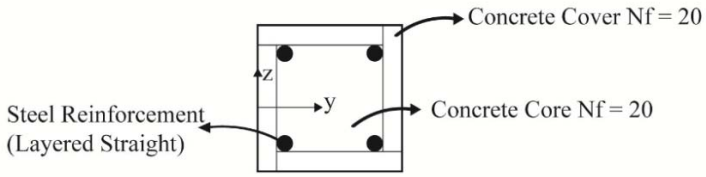

Figure 3: Fibre Discretization of Reinforced Concrete Section

The static stress-strain model developed by Menegotto-Pinto and modified by Filippou et al [13] was used to model the steel rebar behaviour considering strain hardening in steel. Figure 4 (a) shows the complete material constitutive model used for the steel rebar where the experimentally obtained yield stress, ultimate stress and elastic modulus of the rebar were implemented. The reloading and unloading paths in the steel rebar stress-strain relation were adopted from work by Monti and Spacone [14]. The compressive stress-strain envelope for concrete was based on the

model proposed by Mander et al. [15] as shown in Figure 4 (b). The reloading and unloading responses defined by Karsan-Jirsa [16] were implemented. The falling branch of the stress-strain curve in tension was defined by an exponential curve.

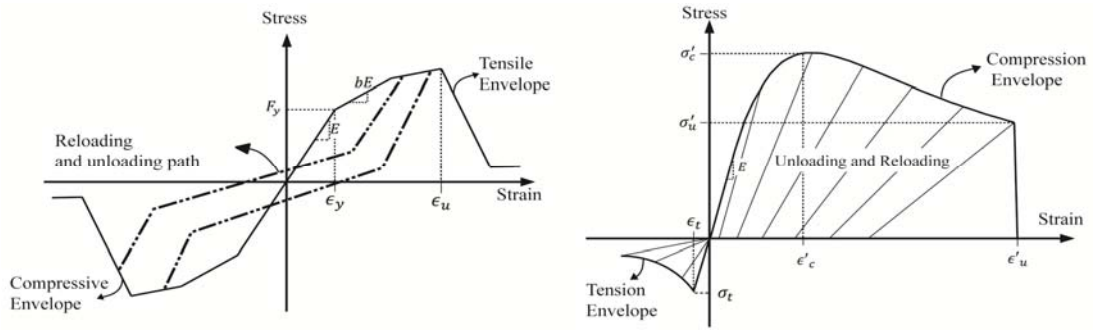

(a) (b)

Figure 4: Stress-Strain Curve; (a) Steel Rebar, (b) Concrete

Modelling of the Masonry Infill Wall

The Shell element, ShellMITC4 [17], was used to model the masonry infill wall. To simulate the stress distribution across the thickness of the masonry infill wall, a multi-layer section, developed by Lu et al. [18], was employed. By discretizing each face-shell of the masonry block into multiple fully-bounded layers in the thickness direction, a multi-layered section of the shell element was used to capture the three-dimensional stress distribution of the masonry infill wall across the flange thickness. Therefore, four shell elements with eight layers modelling both face-shells were used to model a single prism containing a block and mortar. Figure 5 shows mesh size and number of layers used in this study for a single block. The web was not explicitly modelled as the behaviour of the web is believed to be a negligible contributor to the in-plane strength of the infill [12].

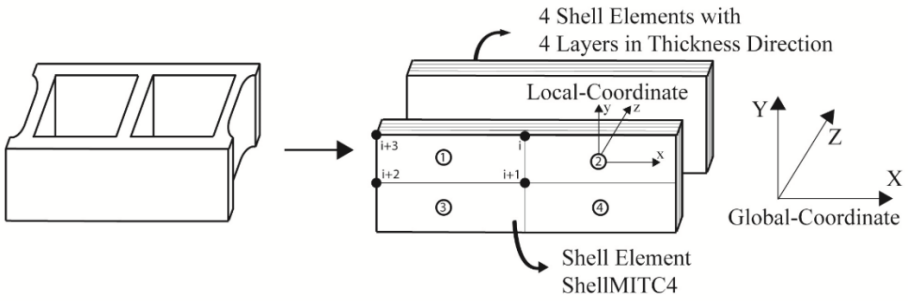

Figure 5: Mesh Size and Number of Layers of Shell Element

The material constitutive model for masonry developed by Lu et al. [18], was employed where both damage mechanics and smeared crack concepts were taken into account. Figure 6 (a) and (b) show the constitutive models used for masonry in tension and compression and Eqns (1) and (2) provide the stress tensor and shear stress, respectively.

$$\sigma_c' = \begin{bmatrix} 1-d_1 & \\ & 1-d_2 \end{bmatrix} D_e \varepsilon_c' \quad (1)$$

$$\tau = \beta G \gamma \quad (2)$$

where σ'_c and ϵ'_c are the stress and strain tensors, respectively; D_e and $d_{i=1,2}$ represent the elastic stiffness matrix, and the damage parameters due to tension and compression, respectively. In the shear stress-strain relation, Eqn (2), β represents the shear retention factor which is used to account for the shear friction between the block and the mortar after sliding occurs.

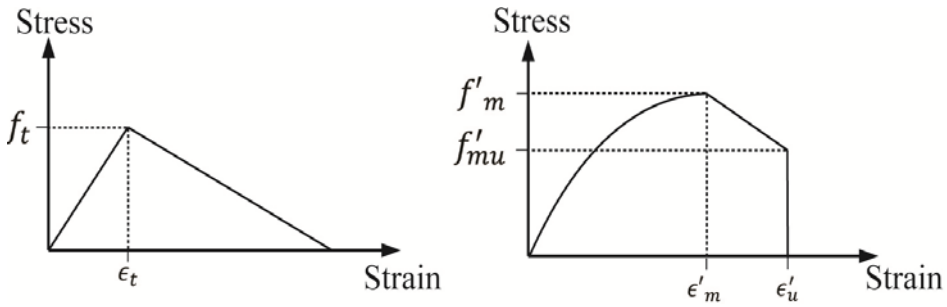

(a) (b)

Figure 6: Smeared Crack Constitutive Model; (a) Tensile Behaviour of Orthotropic Model; and (b) Compressive Behaviour of Orthotropic Model

The interface between the concrete frame and masonry infill wall was modelled using the zero-length element available in OpenSEES. The zero-length element was placed at each point of contact between the masonry infill wall and the bounding frame, connecting the fibre element and the shell element. The zero-length element was assumed to be linear elastic with a high stiffness in compression and practically zero stiffness in tension.

MODEL VALIDATION

Table 2 summarizes experimental and FE results of the ultimate strength and stiffness of each specimen. The strength is determined as the maximum load obtained from either static or hysteretic response curves, and the stiffness is determined as the secant stiffness connecting the maximum load point and the origin. Figure 7 shows the lateral load vs. displacement behaviour of FE versus experimental results for IF-NG under static loading, and BF and IF-TG25 under quasi-static cyclic loading. Note that the response curves of BF and IF-TG25 were backbone curves generated from hysteretic curves of those specimens. As seen from the table, the FE model can predict, with remarkable accuracy, the ultimate strength and stiffness of all specimens for both static and cyclic loading conditions. The figure comparison further shows that the model is also capable of simulating the behaviour throughout a large portion of the loading history. The degradation of stiffness is captured. The difference between experimental and FE results observed at the post-ultimate portion of curves for IF-NG is believed to be due to the actual residual strength of masonry

beyond the ultimate strain. In the model, this strength was considered to be zero but in the experiment, residual stress in the masonry units was observed after the ultimate load was reached.

Table 2: Summary of the Numerical Results vs. Experimental Data

Static Test							Quasi-Static Test						
ID	Strength (kN)			Ultimate Stiffness (kN/mm)			ID	Strength (kN)			Loading Stiffness (kN/mm)		
	F_{exp}	F_{FE}	$\frac{F_{exp}}{F_{FE}}$	K_{exp}	K_{FE}	$\frac{K_{exp}}{K_{FE}}$		F_{exp}	F_{FE}	$\frac{F_{exp}}{F_{FE}}$	K_{exp}	K_{FE}	$\frac{K_{exp}}{K_{FE}}$
BF	58.5	59.1	0.99	1.7	1.7	0.99	BF	60.5	59.8	1.01	1.19	1.16	1.02
IF-NG	133.6	134.9	0.99	12.2	10.2	1.20	IF-FG12	79.5	72.1	1.10	2.52	2.65	0.95
IF-TG7	129.0	133.3	0.97	8.4	8.3	1.02	IF-W-TG12	71.8	64.2	1.12	2.68	2.66	1.01
IF-TG12	102.0	109.1	0.93	3.6	3.5	1.04	IF-TG25	74.5	74.3	1.00	5.54	6.80	0.81
IF-SG7	134.0	129.5	1.03	7.9	6.6	1.19	IF-W-SG12	66.9	70.0	0.96	2.13	1.92	1.11
IF-SG12	114.0	119.6	0.95	2.5	3.1	0.85	-	-	-	-	-	-	-
AVG			0.98			1.05	AVG			1.04			0.98
C.O.V			3.6			12.7	C.O.V			6.7			11.1

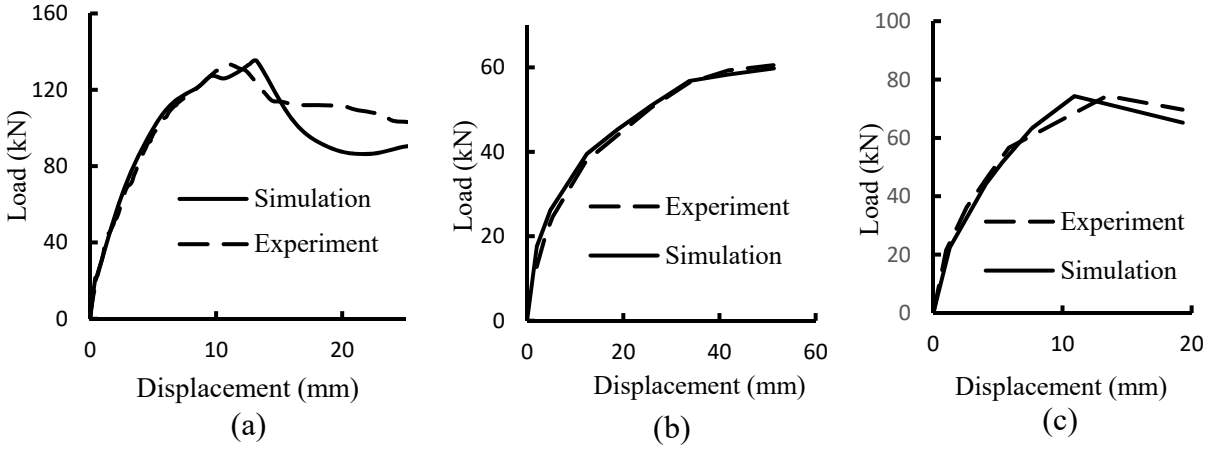

Figure 7: Load vs. Displacement Response of Specimens (a) IF-NG under Static Loading, (b) BF and (c) IF-TG25 under Quasi-Static Cyclic Loading.

RANDOM FIELD SIMULATION OF THE MASONRY COMPRESSIVE STRENGTH

The compressive strength, f'_m, of the masonry prisms was assumed to be lognormally distributed with mean $\mu_{f'm}$, standard deviation $\sigma_{f'm}$, and spatial correlation length $\Theta_{f'm}$. The lognormal distribution is believed reasonable because compressive strength is low-strength dominated and so is well modeled by a geometric average and the geometric average tends to a lognormal distribution by the central limit theorem [8]. Lognormal random fields are fully specified by their mean and covariance structure. A lognormally distributed random field is obtained from a normally distributed random field, $G_{\ln f'm}$, having zero mean, unit variance and spatial correlation length, according to:

$$f'_m(x) = \exp\{\mu_{\ln f'_m} + \sigma_{\ln f'_m} G_{\ln f'_m}(x)\} \tag{3}$$

where x is the spatial position. The mean and standard deviation of the lognormal distribution were obtained from the transformations:

$$\sigma^2_{\ln f'_m} = \ln(1 + V^2_{f'_m}) \tag{4}$$

$$\mu_{\ln f'_m} = \ln(\mu_{f'_m}) - \frac{\sigma^2_{\ln f'_m}}{2} \tag{5}$$

where $V_{f'm}$ is the coefficient of variation of compressive strength. An exponentially decaying (Markovian) correlation function was employed to specify the correlation coefficient between the log-f'_m at a point (x_1) and any other point (x_2) as expressed in the following ([19]):

$$\rho_{\ln f'_m}(\tau) = \exp\left(-\frac{2|\tau|}{\theta_{f'_m}}\right) \tag{6}$$

where τ is the vector between the spatial positions, x_1 and x_2. The spatial correlation length, $\Theta'_{f'm}$, is the distance within which two values of $\ln f'_m$ are significantly correlated. In this random field model, the correlation structure was assumed to be isotropic, so that the correlation length was assumed to have the same length in any direction. Monte-Carlo simulation was then adopted to simulate the random field of the masonry compressive strength. Figure 8 shows an example of a random field realization of the f'_m field, over the masonry infill, where dark colours imply higher masonry prism strength.

LATERAL RESISTANCE DISTRIBUTION OF MASONRY INFILLED FRAMES

The lateral resistance of the masonry infilled frame, denoted as R, is defined as the ultimate in-plane strength of the infilled frame under monotonic loading. In this study, a total of 18 random field simulation runs, comprising of 1000 realizations each, were performed for each of a variety of spatial correlation lengths $\Theta'_{\ln f'm}$, and coefficients of variation of the $\ln f'_m$ field. Table 3

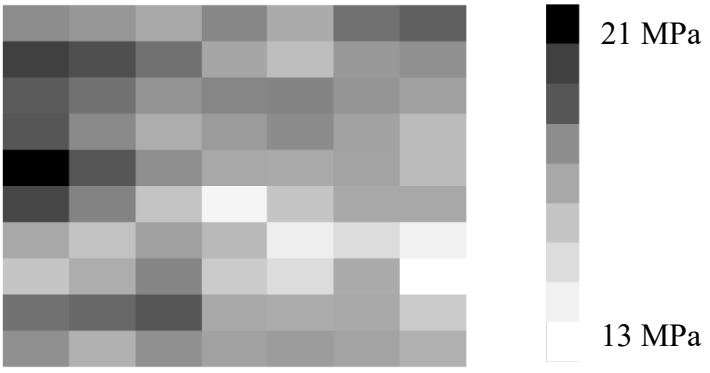

Figure 8: Random Field Simulation of the Masonry Prism Compression Strength.

summarizes these varying parameters. For each simulation, one thousand random fields of f'_m over the infill (one example is shown in Figure 8) were generated. The lateral resistance of the infilled frame for each random field of f'_m was then calculated using the FE model described above. The mean of $\ln f'_m$ was held fixed for all simulation runs, while the coefficient of variation and the correlation lengths were varied as indicated in Table 3. For each simulation set, the resulting estimated mean, μ_R, and standard deviation, σ_R, of the lateral resistance are also shown in Table 3. After 1000 realizations for each simulation set, a resistance histogram was constructed to which a lognormal distribution was fit, an example of which is shown in Figure 9.

It can be seen from Table 3, and further illustrated in Figure 10, that changes in the standard deviation $\sigma'_{\ln f'_m}$ and spatial correlation length of f'_m, $\Theta'_{\ln f'_m}$, did not significantly alter the mean value of the lateral resistance distribution. However, an increase in the standard deviation and spatial correlation length of f'_m results in an increase in the standard deviation of the lateral load

Table 3: Summary of the Random Field and Lateral Resistance Distribution

Random Field ID	Input		output		Random Field ID	Input		output	
	$\theta_{\ln f'_m}$	$V_{\ln f'_m}$	μ_R (kN)	σ_R (kN)		$\theta_{\ln f'_m}$	$V_{\ln f'_m}$	μ_R (kN)	σ_R (kN)
1	0.2	0.10	132.2	3.8	10	2.0	0.20	130.3	8.2
2	1.0	0.10	132.3	5.2	11	5.0	0.20	130.2	10.1
3	2.0	0.10	131.8	5.9	12	10.0	0.20	130.3	10.1
4	5.0	0.10	130.8	7.3	13	0.5	0.30	131.5	7.4
5	10.0	0.10	132.4	7.7	14	1.0	0.30	129.5	8.6
6	2.0	0.15	131.6	7.2	15	5.0	0.30	130.3	12.1
7	0.1	0.20	130.6	4.3	16	2.0	0.30	130.2	9.9
8	0.2	0.20	130.6	5.1	17	10.0	0.30	130.8	12.9
9	1.0	0.20	130.0	7.1	18	2.0	0.50	129.4	13.3

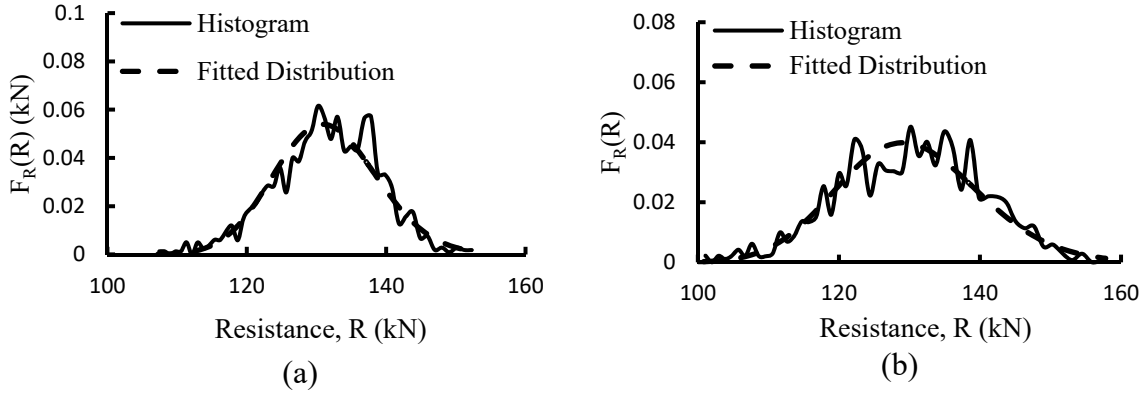

Figure 9: Histogram vs. the Fitted Distribution for Lateral Load Resistance; (a) Random Field ID 12, (b) Random Field ID 10.

resistance. Assuming that the lateral load resistance is normally distributed, the probability of failure for the masonry infilled frame can be calculated as follows, assuming that the load is deterministic, as was done in the study.

$$p_f = \mathrm{P}\left[R < L\right] = \Phi\left(\frac{L - \mu_R}{\sigma_R}\right) \tag{6}$$

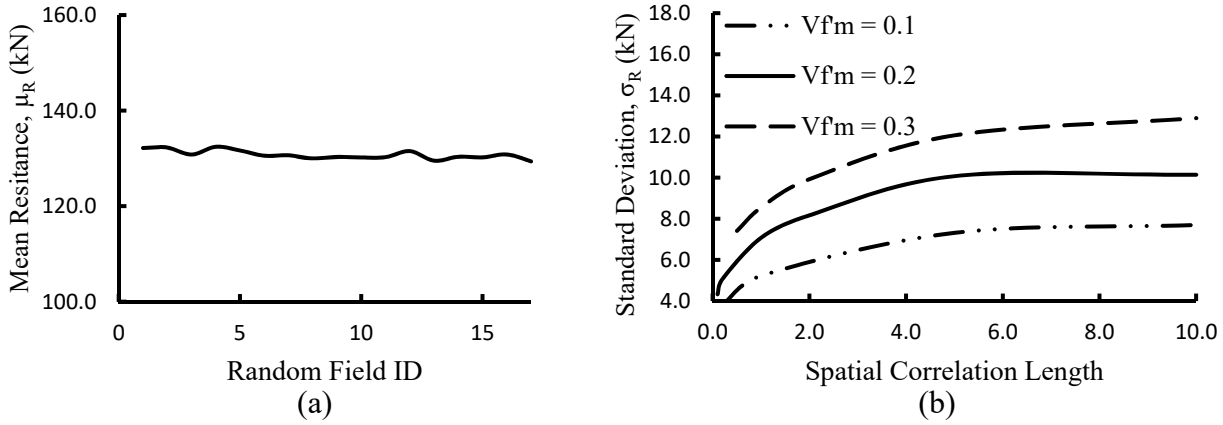

Figure 10: (a) Mean Value of the Lateral Resistance vs. Random Field ID, (b) Standard Deviation of the Lateral Resistance vs. Spatial Correlation length

CONCLUSIONS

A finite element model encoded in OpenSEES was developed to simulate the behaviour of concrete masonry infilled RC frames subjected to in-plane lateral loading. Details of geometric and material models for each component of infilled frame are described in the paper. The model was validated using experimental results for both monotonic and quasi-static cyclic loading. Multiple random field simulations of the masonry prism compression strength were conducted to estimate the distribution of lateral resistance of the masonry infilled frames. It was found that increasing the standard deviation and spatial correlation length of the masonry compressive strength had an insignificant effect on the mean value of the lateral resistance distribution but did result in an increase in the standard deviation of the masonry infilled frame lateral resistance. It is noted that the above conclusions are only applicable to infills of geometric and material conditions described in the paper. Future work should include random field studies with different parameters, such as different infill aspect ratios, interfacial gaps, infill openings, and loading conditions, to ultimately lead to a complete reliability-based design approach for masonry infilled frames.

ACKNOWLEDGMENTS

The authors wish to recognize the contribution of financial assistance by the Canadian Concrete Masonry Producers Association and Natural Sciences and Engineering Research Council of Canada.

REFERENCE

[1] Al-Chaar, G. (2002). "Evaluating strength and stiffness of unreinforced masonry infill structures." *(No. ERDC/CERL-TR-02-1), The U.S. Army Engineer Research and Development Center (ERDC)*, Champaign, Ill.

[2] Hu, C. (2015). "Experimental study of the effect of interfacial gaps on the in-plane behaviour of masonry infilled RC frames." *master's thesis, Dalhousie University*, Halifax, NS, Canada.

[3] Mehrabi, A. B., Shing, B. P., Schuller, M. P. and Noland, J. L. (1996). "Experimental evaluation of masonry-infilled RC frames." *J. of Struct. Eng.*, 122(3), 228-237.

[4] Mosalam, K. M., White, R. N. and Gergely, P. (1997). "Static response of infilled frames using quasi-static experimentation." *J. Struct. Eng.,* 123(11), 1462-1469.

[5] Steeves, R. J. (2017). "Quasi-static testing of masonry infilled RC frames with interfacial gaps." *master's thesis, Dalhousie University*, Halifax, NS, Canada.

[6] Laird, D.A., Drysdale, R.G., Stubbs, D.W., and Sturgeon, G.R. (2005). "The new CSA S304.1-04 Design of masonry structures." *Proc. of the 10th Canadian Masonry Symposium*. Banff, Alberta, 10 p.

[7] CSA S304.1-14. (2014). *Design of masonry structures*. Canadian Standards Association, Ontario, Canada.

[8] Fenton, G. A. and Griffiths, D. V. (2008). *Risk assessment in geotechnical engineering*. 461 pages, Wiley, Hoboken, NJ.

[9] ATC-24, (1994). *Guidelines for cyclic seismic testing of components of steel structures*, Applied Technology Council, Redwood City, CA.

[10] Mazzoni, S., McKenna, F., Scott, M. H. and Fenves, G. L. and others. (2006). "*OpenSees command language manual*," Pacific Earthquake Engineering Research (PEER) Center, Berkeley, CA.

[11] El-Dakhakhni, W., Elgaaly, M. and Hamid, A. A. (2003). "Three-strut model for concrete masonry-infilled steel frames," *J. Struct. Eng.,* 129(2), 177-185.

[12] Hashemi, A. (2007). "Seismic evaluation of reinforced concrete buildings including effects of masonry infill walls" *Doctoral Dissertation, Berekeley University*, Berkeley, CA.

[13] Filippou, F. C., Popov, E. P. and Bertero, V. V. (1983). "Effects of bond deterioration on hysteretic behavior of reinforced concrete joints." *(Report NO. UCB/EERC-83/19), Pacific Earthquake Engineering Research center (PEER)*, Berkeley, CA.

[14] Mander, J. B., Priestley, M. J. N. and Park, R. (1988). "Theoretical stress-strain model for confined concrete." *J. Struct. Eng.,* 114(8), 1804-1825.

[15] Monti, G. and Spacone, E. (2000). "Reinforced concrete fiber beam element with bond-slip." *J. Struct. Eng.,* 126(6), 654-661.

[16] Karsan, I. D. and Jirsa, J. O. (1969). "Behavior of concrete under compressive loading." *J. Struct. Eng.,* ST12(95).

[17] Dvorkin, E. N., Pantuso, D. and Repetto, E. (1995). "A formulation of the MITC4 shell element for finite strain elasto-plastic analysis." J. *Meth. in Appl. Mech. and Eng.,* 125(1), 17-40.

[18] Lu, X. Lu, X. Z., Guan, H. and Ye, L. P. (2013). "Collapse simulation of reinforced concrete high–rise building induced by extreme earthquakes." *J. Earth. Eng. Struct. Dyn.,* 42, 705-723.

[19] Fenton, G. A., Zhang, X. and Griffiths, D. V. (2007). "Reliability of shallow foundations designed against bearing failure using LRFD." *J. Georisk*, 1(4), 202-215.